Surface albedo observations of Hudson Bay (Canada) landfast sea ice during the spring melt

J.K. EHN, M.A. GRANSKOG, T. PAPAKYRIAKOU, R. GALLEY, D.G. BARBER

Centre for Earth Observation Science, University of Manitoba, Winnipeg, Manitoba R3T 2N2, Canada
E-mail: umehnjjk@cc.umanitoba.ca

ABSTRACT. The shortwave albedo is a major component in determining the surface energy balance and thus the evolution of the spring melt cycle. As the melt commences, the ice is partitioned into multiple surface types ranging from highly reflective white ice to absorptive blue ice. The reflectance from these surfaces shows significant spatial and temporal variability. Spectral albedo measurements were made at six different sites encompassing these two surface types, from 19 March to 3 May 2005, on 1.5 m thick landfast sea ice in southwestern Hudson Bay, Canada (58° N). Furthermore, the broadband albedo and the surface energy balance were continuously recorded at a nearby site during the 1 month period. Rapid changes in the albedo were found to relate to typical subarctic climate conditions, i.e. frequent incursions of southerly air, resulting snow and rain events and the generally high maximum solar insolation levels. Subsequently, diurnal variations in snow surface temperature were evident, often causing daytime melting and night-time refreezing resulting in the formation of ice lenses and superimposed ice. After rain events and extensive melting, the snowpack was transformed throughout into melt/freeze metamorphosed snow and superimposed ice. The integrated (350–1050 nm) albedo varied between 0.52 and 0.95 at the blue-ice sites, while it varied between 0.73 and 0.91 at white-ice sites. Variability on the order of ±10% in the white-ice broadband albedo resulted from the diurnal freeze–thaw cycle, but also synoptic weather events, such as snowfall and rain events, could rapidly change the surface conditions.

INTRODUCTION

The ice–albedo feedback mechanism, as a key factor affecting the energy and mass balance of the Arctic, has frequently been emphasized in climate studies (e.g. Curry and others, 1995; Perovich and others, 2002). During the winter, the sea-ice surface albedo is generally high (>0.8) since a layer of dry snow mostly covers the sea ice. With spring, increased shortwave radiation levels result in sufficient absorption within the sea-ice/snow volume to trigger melting and a consequent reduction in albedo. Synoptic weather events, such as inflow of warm air masses and/or rain events, significantly alter the surface albedo (Ohmura, 1982; Robinson and others, 1986). With the advancing melt season, the snow cover gradually disappears and surface melt puddles form. With these changes, the net shortwave radiation contributes an increasing portion of the net radiation at the surface.

Recent albedo investigations in the High Arctic have demonstrated the importance of systematic time-series observations (Perovich and others, 2002). Time-series observations are central to the understanding of the seasonal development of sea-ice/snow covers, and for physical/biogeochemical studies. The Arctic seas exhibit strong seasonal variations in albedo largely due to the sea-ice cover, so any changes in the snow and ice cover would impact the global albedo and thereby influence climate. The subarctic regions are a particularly good place to study the time dependence of radiative exchange due to the strong diurnal forcing in radiation and the advection of warm-air masses which increases temperature and occurrences of rain. A temporal study of radiative exchange at the surface is thus warranted for these subarctic seas, and knowledge gained here may also be useful for near-future arctic conditions if climate variability/change progresses as projected (Johannessen and others, 2004; ACIA, 2005).

SITE DESCRIPTION

We present data collected over a period of 46 days, from 19 March (day of year (YD) 78) to 3 May (YD 123) 2005, on the landfast sea ice in Button Bay (58°48.5′ N, 94°17.2′ W; near Churchill, Manitoba), in western Hudson Bay, Canada (Fig. 1a). The data consist of a continuous record of the sea-ice surface energy balance at a fixed site (Fig. 1b) and a series of spectral albedo measurements at six adjacent locations on the sea ice. The observations were part of a pilot study for theme 3 of ArcticNet (http://www.arcticnet-ulaval.ca). To the best of our knowledge, these are the first-ever such time-series measurements along the western side of Hudson Bay over a typical spring period. In this paper, we describe the surface radiation balance and use the surface temperature as a proxy integrator for the overall surface energy balance.

The ice cover in Hudson Bay is seasonal. The bay becomes fully ice-covered during winter, and ice-free from mid-August to late October (Wang and others, 1994; Gough and others, 2004). In the Churchill region, the ice grows typically 1.3–2.0 m thick and ice break-up occurs on average in early July (Stirling and others, 2004). Under predominantly northwest winds, the ice pack moves to the southeast, removing ice from the northwest and encouraging new ice growth. However, changing winds may rapidly move the mobile pack ice onshore. Strong winds and tidal mixing result in recurring polynyas and leads in the western Hudson Bay. High tides (up to 4 m between low and high water at Churchill port) further aid in breaking up and piling ice floes against the coast or landfast ice boundary. The sea ice in Button Bay thus consisted of a collection of advected ice floes, which during early winter cohered into a continuous landfast ice sheet. Sharp, uneven surface features, rubble fields and pressure ridges were common in the
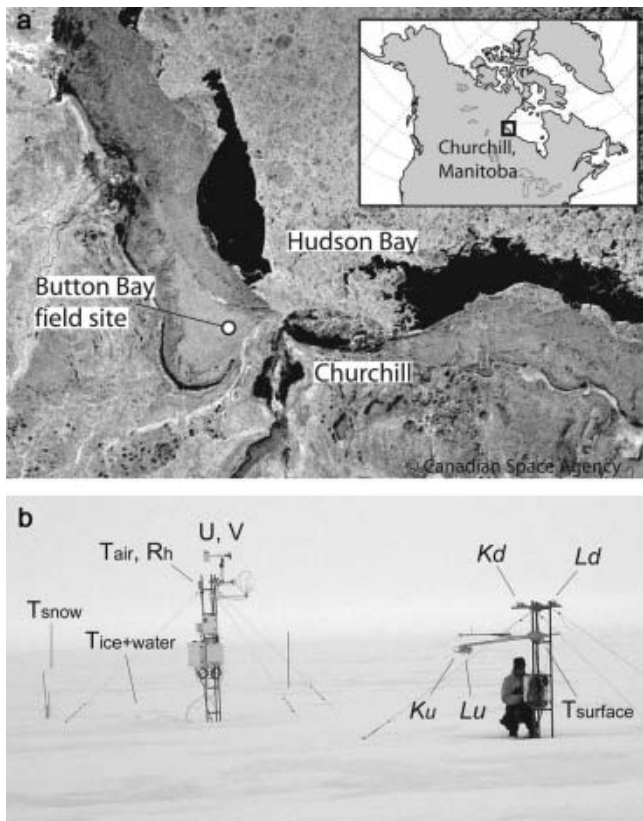
Fig. 1. (a) The Button Bay study area in Hudson Bay, and (b) the surface energy-balance station. The satellite image in (a) is a RADARSAT synthetic aperture radar image taken on 17 April. The surface type surrounding the field site shows the extent of the landfast sea ice. A flaw-lead polynya has formed between the fast-ice edge and the mobile pack. The photograph in (b) was taken on 27 April (YD 117).

area in 2005. However, in order to obtain more representative temporal samples, we located our sampling stations on relatively undeformed ice in Button Bay (Fig. 1b). At the time of the experiment, the level ice reached its maximum thickness of 1.5 m, although large horizontal variability was observed in the area. At the location of the meteorological site, ice thickness increased from roughly 1.2 m to 1.5 m between YD 96 and 123.

Before our field program commenced (i.e. from YD 1 to 78) the air temperature averaged –25°C (Fig. 2a) (National Climate Data and Information Archive, Environment Canada). Two significant low-pressure systems, centered on YD 33 and YD 62, respectively, caused air temperatures to rise above –10°C, and for 2–3 hours even above 0°C in the case of the former. At the start of the experiment, winter conditions prevailed. Air temperatures averaged –19°C. The ice was snow-covered as snow precipitation was ongoing at the time. On YD 87 the snow cover was 0.26 m thick and could generally be characterized as dry snow. These conditions continued about 10 days into the experiment (i.e. YD 88), after which rapid changes in the surface properties occurred. In this paper, we focus on the period that followed (until YD 123), during which the ice evolved from winter conditions to the early stages of melt-pond formation. The oceanic heat flux did not significantly affect the sea-ice energy balance during the measurement period, as the water column below the sea ice was completely

mixed and near the freezing point (unpublished data). The main environmental conditions with effects on the surface albedo were identified as (a) advection of warm air masses, (b) cloud cover, (c) precipitation in solid phase and (d) precipitation in liquid phase.

FIELD OBSERVATIONS

The surface meteorology station at the Button Bay field site was assembled on YD 78 and recovered on YD 123 (Fig. 1b). The monitored parameters included air temperature and relative humidity, wind speed and direction, turbulent fluxes of heat, water vapour, momentum and CO_2 in the atmospheric boundary layer, ice and snow temperatures using thermocouple strings extending through the ice/snow cover, surface skin temperature and the components of the radiation balance. In this study, we focus on the latter two.

The components of the radiation balance are summarized as

$$Q^* = K^* + L^* + K_d - K_u + L_d - L_u, \tag{1}$$

where Q^* is the net all-wave radiation, K^* the net of the incident and reflected shortwave solar radiation (i.e. K_d and K_u) and L^* the net of the incoming and outgoing longwave radiation (i.e. L_d and L_u). Positive net values indicate energy input to the surface.

The radiation balance was measured at 2 s intervals and stored as 15 min averages using two pyranometers (The Eppley Laboratory, Inc., Model PSP, wavelength range 285–2800 nm) and two pyrgeometers (The Eppley Laboratory, Inc., Model PIR, range 3.5–50 μm) for down- and upwelling shortwave and longwave radiation, respectively. The sensors were mounted about 1.5 m above the surface facing south (Fig. 1b). The surface below the radiometers was of the white-ice type (see below). During post-processing, the longwave radiation was corrected for dome and case temperatures using methods described in Marty and others (2003). Frost and water droplets were removed from the sensor domes before 0800 h every morning. For most weather conditions, the sensor domes remained clear from frost or water droplets during daytime, but during rain events it was not possible to keep domes clear and these data may be affected by the water droplets. At the start of the experiment (YD 78), sunrise was around 0630 h local time and sunset around 1830 h. The solar zenith angle was about 78° and 79° at 0800 h and 1700 h, respectively. Thus to reduce measurement errors due to the pyranometers' imperfect cosine response at high zenith angles, broadband albedos were calculated from K_d and K_u data for periods between 0800 and 1700 h (Warren, 1982; Pirazzini, 2004). At the end of the experiment, sunrise and sunset were around 0430 and 1945 h, respectively, and daytime (0800–1700 h) solar zenith angles were smaller than 68°.

Coincident surface skin temperature was obtained at the meteorology station using an infrared temperature transducer (Everest Interscience, Inc., Model 4000.4ZL). The instrument operates in the 8–14 μm spectral range with an accuracy of ±0.5°C and a resolution of 0.1°C for the temperature range –40 to +100°C. It was pointed with a ~45° viewing angle towards the surface below the radiation sensors. The surface temperature is important as it can be regarded as an integrator of surface energy fluxes, i.e. radiation and turbulent fluxes from above and conductive fluxes from below.
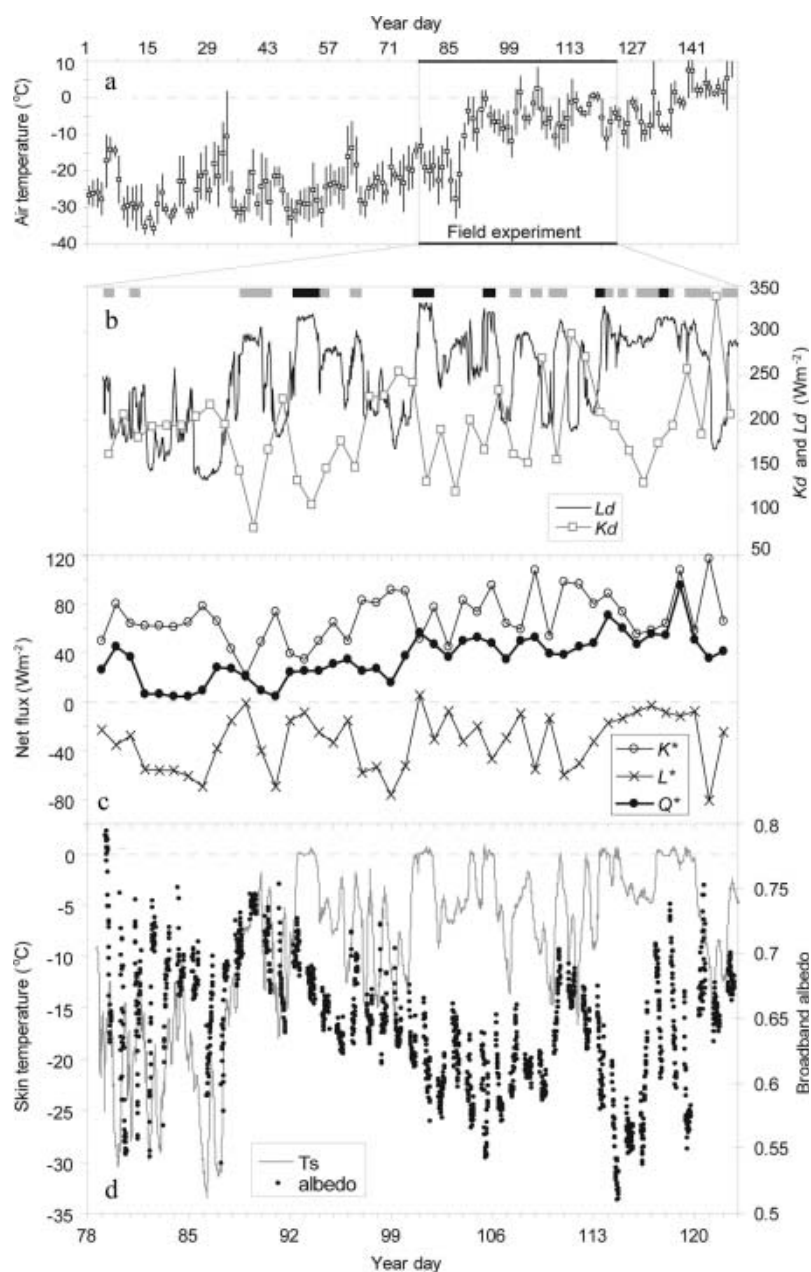
Fig. 2. (a) The daily maximum, mean and minimum air temperatures (T_a) from Churchill (Environment Canada). (b) Hourly averages of incoming longwave radiation (L_d) and daily averages of incoming shortwave radiation (K_d). Also shown in the upper part are the occurrences of snow (grey) and rain (black). (c) Daily averages of the net shortwave (K^*), longwave (L^*) and all-wave (Q^*) radiative energy over the surface. (d) 15 min averages of the surface skin temperature (T_s) and the broadband albedo.

The spectral albedo, $\alpha(\lambda)$, is the fraction of incident irradiance that is backscattered from the surface:

$$\alpha(\lambda) = \frac{K_u(\lambda)}{K_d(\lambda)}, \qquad (2)$$

where λ is the wavelength. The albedo is of interest as it is a measure of solar radiation absorbed by the snow, sea ice and ocean. The wavelength-integrated albedo, α, is commonly used in climatological studies:

$$\alpha = \frac{\int \alpha(\lambda) K_d(\lambda)\,d\lambda}{\int K_d(\lambda)\,d\lambda}. \qquad (3)$$

In this work, we define the wavelength-integrated albedo to have integration limits between 350 and 1050 nm, which are the spectral limits of the dual-headed spectroradiometer (FieldSpec, Analytical Spectral Devices, Inc., Boulder, CO)

used, and the broadband albedo to have integration limits encompassing nearly the entire solar shortwave spectrum, i.e. 285–2800 nm. The spectral albedo was obtained with the spectroradiometer by alternating between up- and downwelling irradiance measurements. The cosine collector was attached to the end of a 1.5 m long rod extending from a tripod. The set-up was kept horizontal about 0.7 m above the surface by using a bubble level. The footprint, from where roughly 90% of the measured upwelling radiation originates, is thus within a circle with a radius double the height above the surface (in case of isotropic incident radiation). A second cosine collector (180° field-of-view) was used for coincident monitoring of changes in incoming spectral irradiance. Spectral albedo was repeatedly measured at six sites considered representative of the area from YD 97 onwards. Three of the sites were classified as blue-ice sites and three
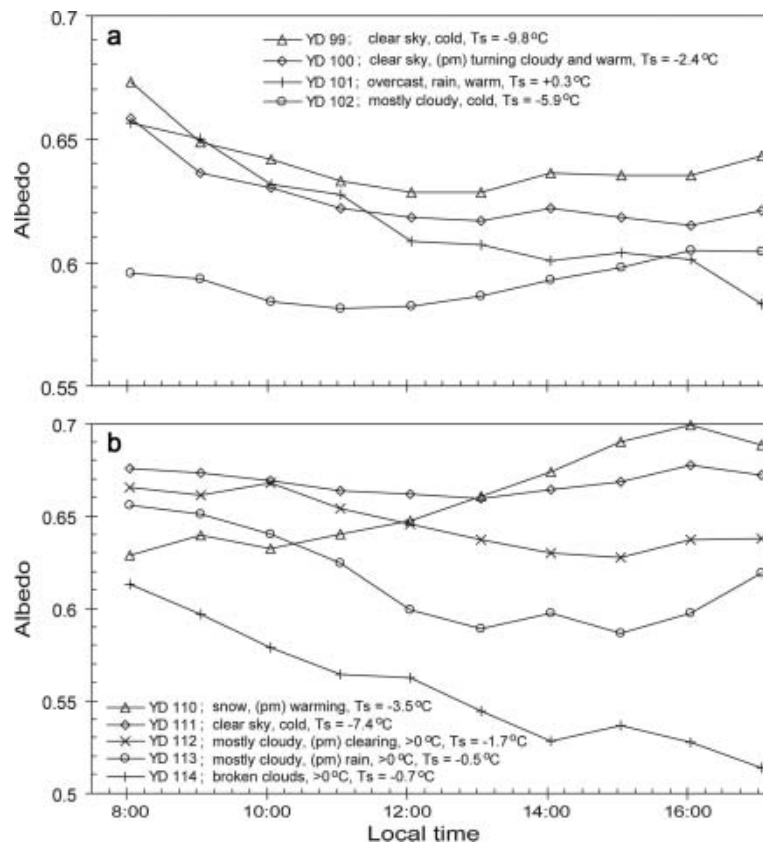
Fig. 3. Daily broadband albedo variations for a sequence of days: (a) YD 99–102; and (b) YD 110–114. Legends show the day of year and prevailing sky and weather conditions. T_s are daily (0800–1700 h) averages of the surface skin temperature.

as white ice. All six sites chosen were large and homogeneously composed of only one ice type. The blue- and white-ice sites thus represented a minimum and maximum albedo in the measurement area. The blue-ice sites tended to lose their snow cover quickly and were darker in appearance than the white-ice sites which appeared white throughout the experiment and formed mounds of snow or drained soft granular ice.

SEASONAL EVOLUTION

From YD 78 to 88, air temperatures remained below –10°C, averaging –19°C. The period shows large variations in the measured broadband albedo due to variable weather conditions (mainly snowfall, snowdrift, freezing fog and cloud coverage). On YD 89, conditions changed dramatically when a low-pressure system moved in, increasing L_d and causing heavy snowfall and freezing rain (Fig. 2). This resulted in a crusty top layer of snow with a density of 413 kg m^{-3} on YD 90, an increase from 366 kg m^{-3} on YD 88. The next low-pressure event occurred 2 days later on YD 92. This time, air temperatures rose above 0°C and with significant rainfall to the surface (28 mm of total precipitation observed at Churchill meteorological station, Environment Canada). Also the surface skin temperature rose above 0°C for the first time in the year (Fig. 2d). Subsequently, ice lenses formed at various levels in the snowpack. Following these synoptic-scale weather events, the broadband albedo dropped from a high of 0.74 (YD 89) to 0.71 (YD 92) and to 0.64 (YD 95) in 6 days (Fig. 2d). These events mark the beginning of the melt season.

Rainfall occurred on five occasions (Fig. 2b). The most significant of these took place around YD 100–101 and was accompanied by thunderstorms. All rain events were marked by increased levels of L_d (Fig. 2b) associated with the cloud cover, increased humidity and warmer air. Recorded values ranged from 310 to 332 W m^{-2}. During snowfall events, L_d was generally below 310 W m^{-2}. As the cloud-covered conditions were accompanied by low levels of K_d, little difference was observed in the daily averaged net all-wave radiation, Q^*; the daily averaged components for K^* and L^* tend to cancel each other out (Fig. 2c). Concurrently there was a subtle seasonal rise in the daily averages of Q^* that may be described by $1.09YD - 74.1$ ($R^2 = 0.52$), while over the same period the slopes for K^* and L^* are 0.64 and 0.45, respectively, with weak correlation ($R^2 = 0.16$ and 0.06). For the duration of the experiment, the net radiative energy balance was positive, i.e. the surface received more radiative energy than it emitted/reflected. Prior to the thunderstorm on YD 100–101, Q^* averaged 21.5 W m^{-2}, and afterwards 50.5 W m^{-2}, an indication of the physical changes that occurred in the snow due to the rain.

After the first rain event and the subsequent formation of ice lenses, measurements of the snow properties were increasingly difficult to conduct. Some sporadic layers between the ice lenses could, however, be measured in the period after YD 101. On YD 101 the density of these individual layers ranged from 250 to 470 kg m^{-3}. Bulk density measurements for the snowpack resulted in 750 kg m^{-3} for a 0.25–0.27 m snow depth on YD 103, and 650 kg m^{-3} for a 0.21 m snow depth on YD 105. By YD 105 the ice surface had fractionated into areas of blue ice and

white ice, i.e. depressed areas of bare ice and mounds with a snow cover over the ice. On this day an up to 1 cm deep layer of meltwater was observed on the bare ice. On YD 110 the snowpack on the white ice was modified all the way through by freeze–thaw processes and composed mostly of ice lenses. The snow/ice interface was difficult to determine as metamorphosed snow formed superimposed ice (based on stable oxygen isotopic composition (unpublished data); see, e.g., Eicken and others, 1994) which merged with the surface ice, causing the interface to become highly uneven. From YD 110, snow temperatures, as measured with the thermocouple strings, were adversely affected by transmitting solar radiation, leaving the surface skin temperature as the best indicator for thermodynamic and metamorphic changes in the snowpack (Fig. 2d).

DIURNAL RADIATIVE PROPERTIES

The daily cycle of broadband albedo showed considerable variations depending on weather conditions. A cloud cover may increase the broadband albedo by up to 10% from clear-sky values by increased absorption in infrared wavelengths (Barry, 1996). Furthermore the albedo is sensitive to metamorphic changes in the snowpack, such as grain size and liquid-water content (Warren, 1982). During the melt season these properties change rapidly. In this section, we examine the daytime evolution of the white-ice albedo related to cloud and surface conditions.

The diurnal trends in sea-ice/snow surface properties for the melt period were characterized by a daily-thaw/night-time-refreeze cycle. The surface skin temperature decreased during the night and showed a daytime low in the morning (Fig. 2d). During the day, surface temperatures increased, reaching the melting point. At the same time the broadband albedo decreased during the day in response to the freeze–thaw cycle (Fig. 2d). During the night the surface refroze, resulting in an albedo increase.

Superimposed on the daily decreasing trend are effects from the sky conditions on the broadband albedo. Under clear sky, the albedo decreased during the course of the day. Minimum values were reached in the early afternoon, after which increasing values were observed (e.g. YD 99, 100 and 111 in Fig. 3). This increase can be attributed to decreasing solar zenith angles and decreasing K_d when the direct component of the K_d dominates (Pirazzini, 2004). Under overcast conditions, the zenith angle has a smaller effect on albedo, as K_d is mainly composed of diffuse radiation. When L_d is increased by the cloud coverage, no substantial decrease in all-wave energy input to the surface is observed. Furthermore, during an overcast sky, air temperatures tend to be higher than during clear-sky conditions. Thus through the course of the day the albedo shows a stronger decrease under overcast conditions compared to clear-sky (Fig. 3).

The snow event on YD 110, with the drop in air temperatures, briefly increased the broadband albedo to ~0.7 (Figs 2d and 3b). The density of the new snow varied from 165 to 180 kg m^{-3}. However, the new snow was short-lived as the warm temperatures that followed quickly caused extensive melt. Consequently the albedo abruptly dropped to 0.51, the lowest observed value during the experiment. The abrupt effect of snow and rain events is illustrated in Figure 3b. The snowfall on YD 110 caused a daytime (0800–1700 h) increase in albedo by 0.07 or 11%, while the effect of the rain and the warm weather on YD 114 decreased the
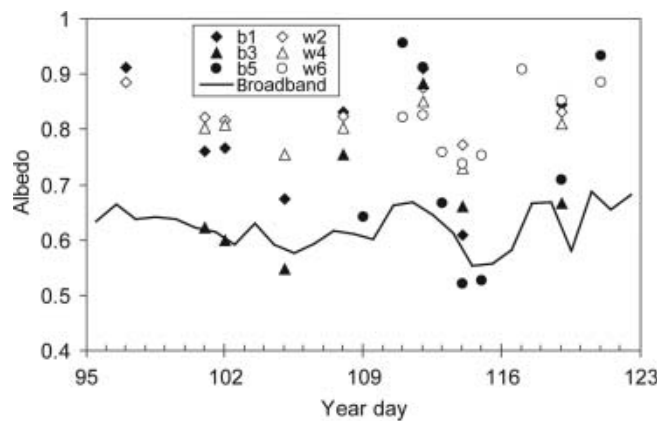

Fig. 4. Time series of the wavelength-integrated albedo at three blue-ice (b1, b3, b5) and three white-ice sites (w2, w4, w6), and the daily averaged broadband albedo at the surface meteorology station (white ice).

albedo by 0.1 or 16%. The rate of decrease of albedo during the 5 day period was −0.047 d^{-1}. Such rapid changes were also observed over multiyear ice during the melt period by Perovich and others (2002). In general, the daytime change in the broadband albedo over white ice ranged from a 0.01 h^{-1} increase to a decrease of 0.014 h^{-1}.

SPECTRAL ALBEDO

The spatial and temporal variability of the broadband- and wavelength-integrated albedo is illustrated in Figure 4. On YD 97 the surface looked spatially uniform due to recent snowfall. The snow depth at the albedo sites was 0.08–0.28 m. The surface was covered with a 2–3 mm thick new snow layer above a hard crust. Consequently the integrated albedos were near 0.9 (Fig. 4). At this point, differences in surface elevation already revealed where melt ponds were likely to form. By YD 101, albedo had decreased to ~0.8 at the sites of the previous measurements (b1 and w2). The albedo was dominated by the wet snow cover; at b1 and w2, snow depth had decreased by about 0.04 m. However, the melt had progressed more rapidly at b3 where the albedo was measured over a 0.05 m thick, very wet and patchy snow surface. At b3 the albedo had reduced to 0.62 and most likely represents the minimum in the area. On YD 105 the surface had fractionated into bare blue ice and snow-covered white ice. The blue-ice areas had a lower elevation than the white ice, which appeared as mounds. On the surface of b1 was a 1 cm thick slushy and dark snow layer, while b3 had a 1 cm deep meltwater layer with small roughness elements protruding above the surface. Minimum albedos were related to warm days when the surface temperature rose to the melting point. The lowest albedo for both the blue and the white ice was observed around YD 113–115 (Fig. 4).

During the following days, snowfall and snowdrift increased the surface albedo. For the blue ice the highest integrated albedo (0.95) was observed on YD 111, when the daily averaged air temperature was −9°C and a 0.06 m new snow layer (with a density of 160–180 kg m^{-3}) covered the surface. Similarly the high values for white ice occurred on YD 121, when snowfall from the day before, clear skies and a cold spell depressed the surface temperature below −10°C.
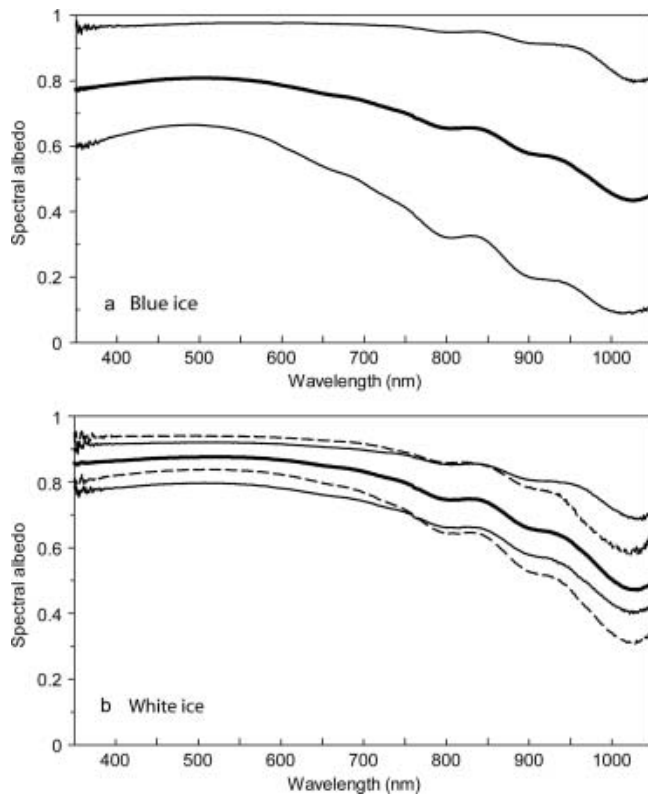
Fig. 5. Spectral albedos of (a) blue ice and (b) white ice from YD 97 to 121. The thick lines are the averages for three sites each during the sampling period, while the thin lines show the extremes. In (a) the maximum albedo was observed on YD 111 and the minimum on YD 115. In (b) the maximum albedo for $\lambda < 845$ nm (dashed line) was observed on YD 117 and for $\lambda > 845$ nm (solid line) on YD 121. The minimum for $\lambda < 767$ nm (solid line) was found on YD 114 and for $\lambda > 767$ nm (dashed line) on YD 113.

Interestingly, areas of blue ice (early stages of melt ponds) caught more of the snow due to larger surface roughness compared to white-ice mounds where the snow cover was more affected by erosion by wind. The albedo for blue-ice areas thus rose to higher values than the white ice after snow events (Fig. 4; YD 111–112 and 121). However, the initially determined locations for depressions and mounds remained the same once the new snow melted.

The magnitude and shape of the spectral albedo was similar to spectra obtained during the melt season in the Arctic (e.g. Grenfell and Perovich, 1984). High values observed after snow events show little spectral dependence in the visible and a modest decrease towards near-infrared wavelengths (Fig. 5). Minimum albedos that occurred as a result of warm days and rain events show considerably more wavelength dependence. A local maximum is observed at 500 nm and a considerable decrease with wavelength by up to 0.6 or 86% (Fig. 5a).

The effect of liquid water present on the surface on the spectral shape is illustrated by the albedo extremes in Figure 5b. The albedo at infrared wavelengths is very sensitive to liquid-water content which greatly increases absorption and reduces scattering (Grenfell and Perovich, 1984). On YD 117 after the snow event, a 0.06–0.07 m thick, wet new snow layer covered the old snow surface. Surface temperatures were at the melting point (Fig. 2d). Consequently the albedo decreased substantially in the near

infrared. The albedo during the clear, cold conditions on YD 121 (see above), on the other hand, shows significantly less wavelength dependence. The spectral differences between YD 113 and 114 are more indicative of spatial variability in the snowpack; the broadband albedo on YD 114 is smaller than on YD 113 (Fig. 3b), while the spectral shape for the albedo for YD 113 would suggest lower broadband values.

CONCLUSIONS

The seasonal evolution of the landfast sea-ice surface albedo in Button Bay was found to be affected by synoptic weather events that caused abrupt fluctuations in values (Fig. 2d). These events can be summarized as (a) advection of warm air masses, (b) cloud cover, (c) precipitation in solid phase, and (d) precipitation in liquid phase. In general, the albedo was spatially fairly uniform during winter. As melting progressed, the overall albedo decreased and spatial variability increased. The surface partitioned into regions of highly reflective white ice and absorptive blue ice.

The effect of cloud cover was to decrease K_d and increase L_d. Their combined effect was thus to even out the radiative energy input to the surface along the day, although the daily average Q^* showed little change. When cloudy conditions were correlated with high air temperatures, extensive surface melting caused the albedo to decrease throughout the day (Fig. 3). In contrast, clear skies resulted in daytime melting and a consequent reduction in albedo, but in the afternoon the surface began refreezing and the albedo increased.

Climate forecasts using global climate models indicate that we should expect a warmer, wetter winter season in the Arctic regions (Johannessen and others, 2004; ACIA, 2005). Our observations during a subarctic spring provide a glimpse of the surface radiation budget's response to such conditions. Rain events caused a rapid change in the snow-cover properties and caused a non-recoverable decrease in the surface albedo due to metamorphoses in the snowpack. Snowfall temporarily increased the albedo by about 0.1, but with the return of warm weather the effect was brief. The precipitation events caused diurnal changes in the albedo of roughly ±10%. These results are similar to those observed by Perovich and others (2002) during the SHEBA (Surface Heat Budget of the Arctic Ocean program) field experiment in the Arctic basin.

REFERENCES

Arctic Climate Impact Assessment (ACIA). 2005. *Arctic Climate Impact Assessment – scientific report.* Cambridge, etc., Cambridge University Press.

Barry, R.G. 1996. The parameterization of surface albedo for sea ice and its snow cover. *Progr. Phys. Geogr.,* **20**(1), 63–79.

Curry, J.A., J.L. Schramm and E.E. Ebert. 1995. Sea ice–albedo climate feedback mechanism. *J. Climate,* **8**(2), 240–247.

Eicken, H., M.A. Lange, H.W. Hubberten and P. Wadhams. 1994. Characteristics and distribution patterns of snow and meteoric ice in the Weddell Sea and their contribution to the mass balance of sea ice. *Ann. Geophys.,* **12**(1), 80–93.

Gough, W.A., A.R. Cornwell and L.J.S. Tsuji. 2004. Trends in seasonal sea ice duration in southwestern Hudson Bay. *Arctic,* **57**(3), 299–305.

Grenfell, T.C. and D.K. Perovich. 1984. Spectral albedos of sea ice and incident solar irradiance in the southern Beaufort Sea. *J. Geophys. Res.,* **89**(C3), 3573–3580.

Johannessen, O.M. *and 11 others.* 2004. Arctic climate change: observed and modeled temperature and sea-ice variability. *Tellus,* **56A**(4), 328–341.

Marty, C. *and 9 others.* 2003. Downward longwave irradiance uncertainty under arctic atmospheres: measurements and modeling. *J. Geophys. Res.,* **108**(D12), 4358. (10.1029/2002JD002937.)

Ohmura, A. 1982. Climate and energy balance on the Arctic tundra. *J. Climatol.,* **2**(1), 65–84.

Perovich, D.K., T.C. Grenfell, B. Light and P.V. Hobbs. 2002. Seasonal evolution of the albedo of multiyear Arctic sea ice. *J. Geophys. Res.,* **107**(C10), 8044. (10.1029/2000JC000438.)

Pirazzini, R. 2004. Surface albedo measurements over Antarctic sites in summer. *J. Geophys. Res.,* **109**(D20), D20118. (10.1029/2004JD004617.)

Robinson, D.A., G. Scharfen, M.C. Serreze, G. Kukla and R.G. Barry. 1986. Snow melt and surface albedo in the Arctic basin. *Geophys. Res. Lett.,* **13**(9), 945–948.

Stirling, I., N.J. Lunn, J. Lacozza, C. Elliott and M. Obbard. 2004. Polar bear distribution and abundance on the southwestern Hudson Bay coast during open water season, in relation to population trends and annual ice patterns. *Arctic,* **57**(1), 15–26.

Wang, J., L.A. Mysak and R.G. Ingram. 1994. Interannual variability of sea-ice cover in Hudson Bay, Baffin Bay and the Labrador Sea. *Atmos.–Ocean,* **32**(2), 421–447.

Warren, S.G. 1982. Optical properties of snow. *Rev. Geophys. Space Phys.,* **20**(1), 67–89.